A Wirelessly Controlled Shape-Memory Alloy-Based Bistable Metal Swimming Device

Yu Wan[1], Keith Cuff[1], and Michael J. Serpe[1]

[1]Affiliation not available

January 12, 2022

Abstract

Shape memory Nitinol has long been used for actuation. However, utilizing Nitinol to fabricate novel devices for various applications is a challenge, but has shown incredible promise and impacts. Bistable metal strips are widely adopted for shape morphing purposes (primarily in kid's toys, e.g., snap bracelets) due to their easy and robust transformation between two states. In this paper, we combine Nitinol shape memory alloy and bistable metal strip to fabricate a swimming actuator with both slow moving and fast snapping capability, akin to an octopus swimming slowly in water, but quickly moving upon encountering a threat. The actuator developed here can also swim in multiple directions, all controlled by a wireless module. Furthermore, we demonstrate that an on-board sensor can be incorporated for potential environmental monitoring applications. Taken together, along with the fact that the device developed here has no mechanical parts, makes this an interesting potential alternative to more expensive, and energy consuming boats.

Corresponding author(s) Email: *serpe@ualberta.ca*

ToC Figure

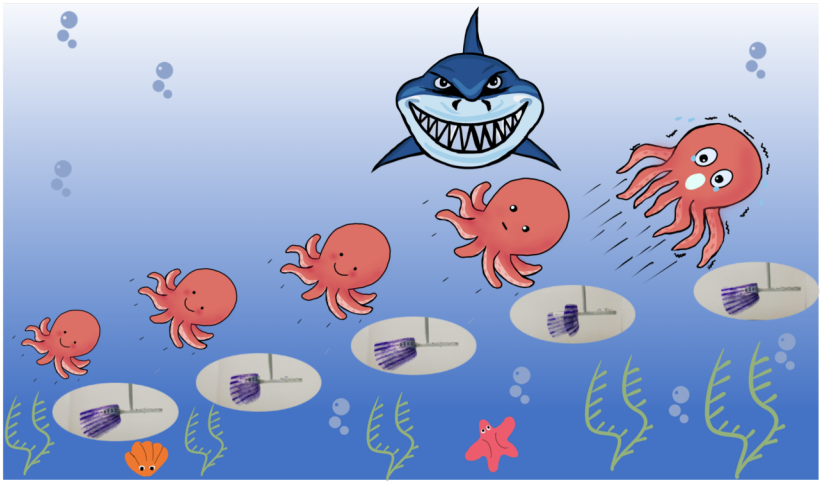

Figure 1: **ToC Figure. A biomimetic swimming actuator inspired by octopus is fabricated.** The actuator utilizes shape memory alloy Nitinol and bistable metal strip to realize repetitive actuation for both slow moving and fast snapping mimicking how octopus can swim carefree and spurt away to escape predators. With wireless module and standalone battery, the actuator is programmable and can be control remotely.

Introduction

For centuries, humans have been fascinated with studying nature and natural processes; this most certainly began out of curiosity, although in many cases led to a desire for mimicry (Whitesides, 2015) (Baytekin et al., 2018) (Aubin et al., 2019). For example, primitive, early humans would move, dress, and act like animals to improve their hunting successes, while modern day mimicry is focused on the development of new synthetic materials for improving human health, and quality of life (Li et al., 2018) (Dang et al., 2018). Of course, nature has the ability to adapt to changes in environmental conditions and added pressures via many years and generations of evolution, while humans are left primarily using rational thought, science, and engineering for adaptation. A great example of nature adapting to their environment for self-gain is the octopus. The octopus is an intelligent marine creature that has evolved the ability to change color and eject ink when in danger in order to escape and preserve its wellbeing. Octopus also exhibit high dexterity, capable of reaching (Cianchetti et al., 2011), grabbing (Cianchetti et al., 2015), swimming (Kazakidi et al., 2015), and walking (Calisti et al., 2015). Interestingly, they have the ability to swim slowly to disguise themselves as floating algae in ocean currents, while maintaining the ability to quickly swim away in a moment by contracting their bodies and whipping their tentacles. Here, we introduce a device composed Nitinol wire (a shape memory material), and bistable metal strips, to generate a device that is capable of mimicking the swimming behavior of an octopus by exhibiting the ability to swim slow and "instantaneously" fast by simply changing how the device's components are electrically stimulated.

Nitinol, generated by alloying nickel and titanium, has many interesting uses and properties, e.g., shape memory, superelasticity, anticorrosion, and biocompatibility (Duerig et al., 1999). As a result of these interesting properties and attributes, it has long been used for applications in aeronautical and space technologies, automobile industries, medical devices and civilian products (Kauffman and Mayo, 1997). Of importance to this investigation is Nitinol's shape memory properties, which we propose harnessing for this new approach to actuation. Nitinol can be "trained" to adopt a desired permanent shape when it's fixed, heated above the austenite finish temperature (Af) and then rapidly cooled to below the martensite finish temperature (Mf) (Liu and Xie, 2007). Below Mf, the Nitinol can be reshaped into temporary shapes and upon heating to above the austenite start temperature (As), a phase transition from martensite to austenite is initiated,

and the Nitinol starts to recover its permanent shape. Importantly, when the temperature is lowered to martensite start temperature (Ms), the Nitinol then can be reshaped again. This shape memory behavior is key to our actuation device. Heating of Nitinol can be achieved by direct heating, or via resistive/Joule heating by applying a voltage to the wire that generates a subsequent current. For this study, we were interested in using Joule heating to trigger the shape memory behavior from the Nitinol.

Bistable materials are known to exist in two stable states that could differ in conformation dramatically. Very common examples of bistable materials are slap bracelets (a child's toy) and metal measuring tapes. In these examples, an external stimulus (force) can be used to trigger the metal strip to quickly morph from one stable state (e.g., extended state) to the other (e.g., coiled state) in what is often called "snap-through" behavior (Ye and Pellegrino, 2005). This sudden and powerful actuation is intriguing if it can be harnessed and utilized – in our case for shape changing devices (Cazottes et al., 2008) (Rothemund et al., 2018) that can be used for swimming.

In this work, we propose harnessing the power of shape memory materials for actuation (and ultimately swimming) by coupling Nitinol wire to bistable materials in a device. By combining these two classes of materials in a device, and utilizing the actuation afforded by Nitinol and the snapping power of bistable metal strips, we developed a novel actuator that mimics the slow and fast swimming behavior of an octopus. Furthermore, by controlling and moving the arms independently (via electrical stimulation), the device can navigate through space in any direction. Additionally, a wireless control system, equipped with a rechargeable battery, was designed to make the device totally autonomous, and untethered from external wires that otherwise would be needed for control. Finally, we demonstrate that we can integrate etalon-based sensing devices (Sorrell and Serpe, 2011) into the construct to monitor water pH and ionic strength. In this case, the etalons tethered to the swimming device change color (that can be captured with an on-board camera) as the water properties change. Successful integration of these sensing devices into the construct demonstrates the potential utility of these devices for environmental monitoring applications, as well as others.

Results and Discussion

For this study, in order to generate devices capable of exhibiting slow and fast swimming behavior upon electrical stimulation, the power of Nitinol and bistable strips needed to be harnessed using careful device design principles. The design we converged on after many iterations is shown schematically in **Figure 2**. As can be seen, four pieces of pre-set short helical Nitinol wires were stretched and attached to the tip of a bistable metal strip. When a voltage was applied to the Nitinol wires, e.g., the front left (FL) piece, the FL Nitinol wire heats up and will shorten thus pulling the tip of the bistable metal strip causing it to snap and coil (trigger process). This snapping process results in lengthening/straightening of the back left (BL) Nitinol wire. The shortening/contraction of the BL Nitinol wire can further be triggered by application of a voltage/heat pulling the tip of the bistable metal strip to uncoil and return to a flat state (reset process). This reset process once again lengthens the FL Nitinol, which prepares the device for its next trigger process. Thus, by carefully (and independently) controlling the conformational state of the four pieces of Nitinol wires with voltage, the state of the bistable strip can be manipulated and controlled allowing slow and fast movement of the device's arms, much like the control an octopus has over its tentacles. Although, to understand how all of the pieces of the device work together to achieve the desired behavior, a detailed examination of the device's components is required, as detailed below.

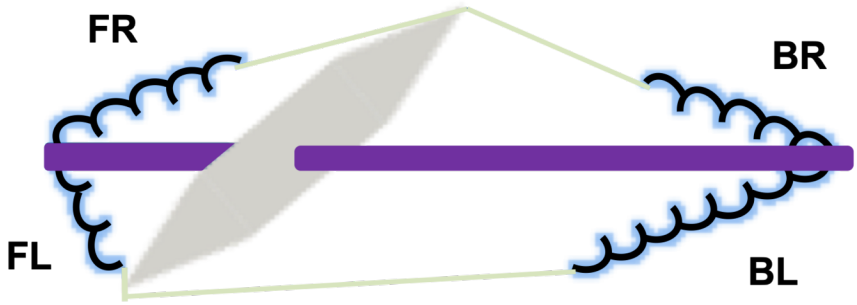

Figure 2: Conceptual design of the swimming device. Grey piece is a bistable metal strip; black coils are Nitinol wires (FL: front left; FR: front right; BL: back left; BR: back right); blue highlights around the coils are hydrogels; purple rod is a central pivot supporting plastic piece; light green lines connecting metal strip and nitinol coils are nonelastic threads.

2.1. Bistable Metal Strip

2.1.1. Metal Strip Shape and Trigger/Reset Angle

Initial studies focused on investigating how the shape of the bistable metal strip and trigger/reset angles impacted its triggering and resetting force. Here, "trigger force" refers to the force required to cause the bistable metal strip to rapidly coil, doing work in the process. "Reset force" refers to the force required to bring the bistable metal strip back to its extended state so that it is ready to be triggered again. In terms of "shape", we focused on changing the taper ratios of the bistable metal strips, while fixing the total length, as shown in **Figure 3**. To measure the forces generated from the snapping action of the bistable strip, an inelastic thread attached to the tip of the bistable metal strip was attached to a force detector, and the trigger/reset forces were measured by pulling the thread (**Figure 4**). When the thread was pulled, a force-time curve was recorded as shown in **Figure S1**, indicating how forces evolved during the trigger/reset processes. Different pulling rates were tested and we found pulling rates had no effect on the minimum force required for trigger and reset (**Figure S2**). A pulling rate of ˜5 cm/s was chosen for these experiments due to ease of reproducibility of this rate. The minimum forces required for trigger and reset were plotted against the taper ratio. We concluded from the data in **Figure 5** that bistable metal strips with larger taper ratios yielded smaller trigger and reset forces. When the metal strip had a larger taper ratio, we noticed a flatter surface at the tip, which results in easier actuation due to smaller force required to transform the tip from one curvature to the other.

Meanwhile, we investigated how the angle that the force was applied to the bistable metal strip, via the thread, impacted the magnitude of the trigger and reset forces. As shown in Figure 3, using the extended state of the bistable metal strip as a reference, we varied the angle of force application to trigger/reset the bistable metal strips. Three different angles were investigated for both the trigger and reset processes. As can be seen in **Figure 6**, larger trigger/reset angles led to smaller forces required for triggering and resetting. This could be explained from the force analyses of the process. When the angle of the applied force is large, the effective normal force, which is the projection of the vector force applied onto the tip of the metal, is likewise large. As a result, if the normal force required to trigger or reset the metal strip remains the same, larger angles lead to smaller vector force required. From the result, we concluded that we can minimize the force by maximizing the angle of force application approaching 90°. However, the angle was limited by the actual reasonable dimensions of the device. For our device design, considering the dimensional constraints and aesthetic aspects, we used 45° for triggering and 60° for resetting.

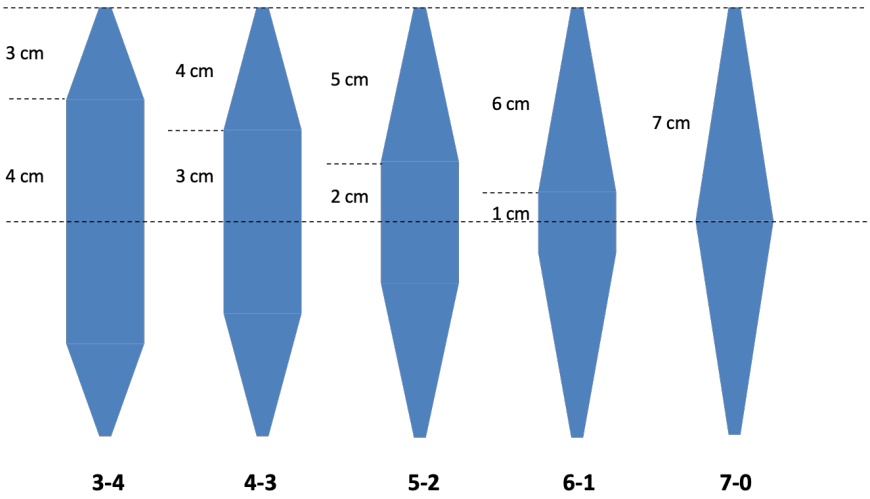

Figure 3: Different shape designs of the bistable metal strips. The tips were tapered to a different extent. From left to right, the taper ratio becomes larger. The number below represents the shape of the strip: taper ratio (First number: tapered length; second number: untapered length).

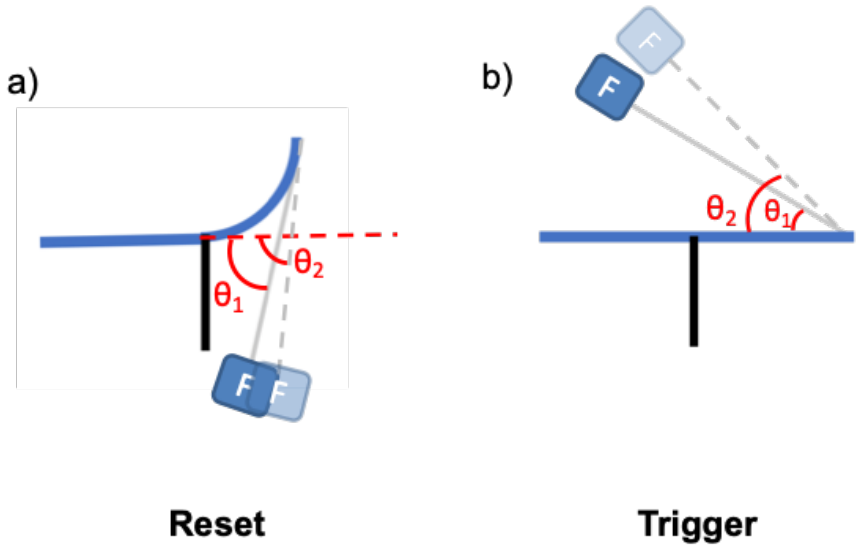

Figure 4: Side view illustration of **a)** reset and **b)** trigger force tests. The angles are all in reference to the extended position of the metal strip. Theoretically, the angle (ϑ) can range from 0° to 180°. However, restricted by the device design, the angle is below 90°. (Blue: bistable metal strip; black: pivot fixed onto the middle of the metal strip; silver: pulling thread; box with "F": force sensor)

2.1.2. Energy Output

While the above investigation revealed the impact of the taper ratio of the bistable metal strip on the trigger and rest forces, it also revealed that the taper ratio impacted the energy that can be generated as a result of the snapping process. To further understand the relationship between snapping energy output and taper ratio, we performed energy output tests. Specifically, the benefit of using bistable metal strips for device

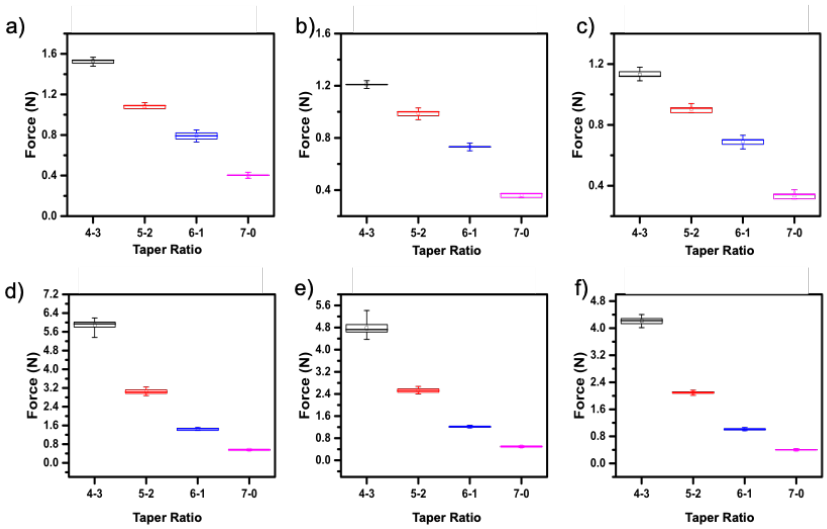

Figure 5: Boxplot of reset forces for different taper ratios at certain trigger/reset angles **a)** 50°, **b)** 60°, and **c)** 70°. Box plot of trigger forces for different taper ratios at certain trigger/reset angles **d)** 25° **e)** 35°, and **f)** 45°. For all the angles, both reset and trigger forces decrease with more tapering on the tip.

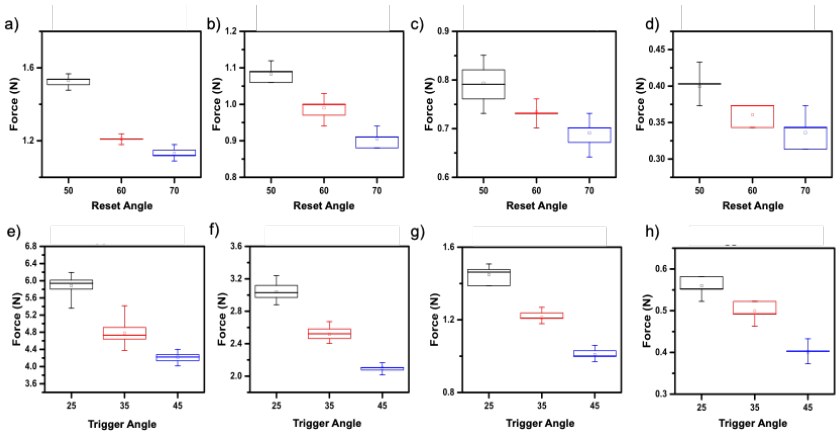

Figure 6: Boxplot of reset forces with different angles at certain taper ratios **a)** 4-3, **b)** 5-2, **c)** 6-1, and **d)** 7-0. Box plot of trigger forces with different taper ratios at certain angles **e)** 4-3, **f)** 5-2, **g)** 6-1, and **h)** 7-0. For all the taper ratios, both reset and trigger forces decrease with larger angle.

propulsion is its fast and powerful snapping behavior, which hypothesized would lead to fast movement of the device developed here. Hence, we wanted to retain good snapping performance while minimizing the magnitude of the trigger and reset forces. To accomplish this, we used a regular ping pong ball that was hung over the top side of the bistable metal strip as shown in **Figure S3**. By triggering the tip of the bistable metal strip, the strip snapped, coiled, and struck the center of the ping pong ball, sending it into motion. The ping pong ball then moved in a circular path, like a pendulum, and eventually reached its highest point before swinging back. Assuming no energy loss during the process, the energy output of the bistable metal strip is directly proportional to the maximum height the ping pong ball reached. Analysis of the height the ping pong ball reached as a function of the bistable metal strip taper ratio allowed us to determine the relationship between energy generation and bistable metal strip taper ratio. As shown in **Figure 7**, the height the ping pong ball can reach (and the energy generated) greatly decreased with larger taper ratios;

i.e., larger taper ratios yielded lower snapping energy output. In fact, the 7-0 taper ratio metal strip did not have enough energy to move the ping pong ball. Since snapping energy is essential to the performance of the swimming device, we decided to maximize the energy output by adopting a 4-3 taper ratio design for our future devices.

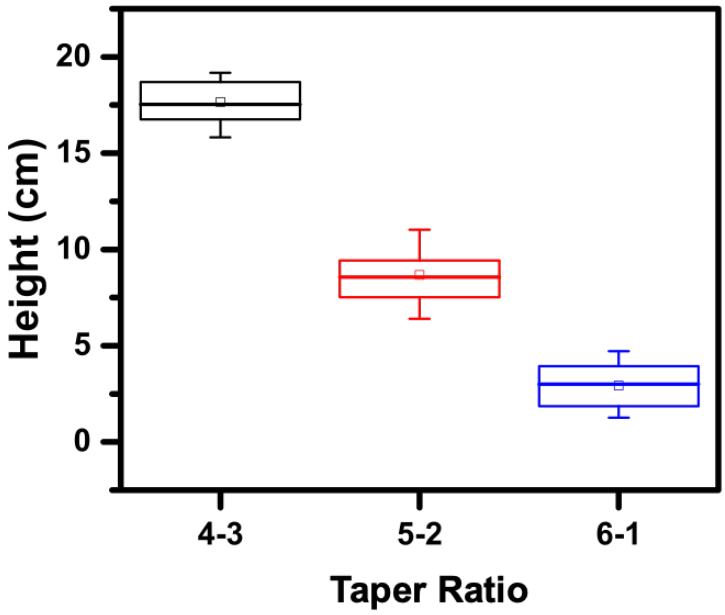

Figure 7: Snapping energy of different taper ratios. The figure shows the height the ping pong ball reached for different taper ratios. 7-0 is not included here because the snapping is difficult to reproduce and didn't have enough force to move the ping pong ball.

2.2. Nitinol Wire

2.2.1. Phase Transition Temperature

We first investigated the phase transition process using differential scanning calorimetry (DSC), as shown in **Figure S4**. From the DSC, we observed the phase transition to be ˜60 . We also performed a water bath test on the Nitinol (**Figure S5**(a)). Specifically, the Nitinol was set into a helical structure (contracted state) in a furnace and subsequently stretched into an extended state. Then, the extended Nitinol wire was immersed into a beaker of water for ten seconds at various temperatures and taken out for length determination. From the data (Figure Figure S5(b)), we observed a sharp length change at ˜60 , which was consistent with the DSC test.

2.2.2 Actuation Force Output at Different Voltages

The forces the Nitinol wire can exert upon temperature-induced contraction/shortening determines its ability to apply force to the bistable metal strip for triggering and resetting. Hence, we investigated the force output of the Nitinol wire when stimulated to contract upon application of a voltage, which induced a temperature change above the phase transition temperature. For these experiments, the Nitinol wire was connected to a force sensor, and was not allowed to contract upon stimulation (**Figure S6**(a)). Different voltages were applied until the force reached 4.2 N, which was the minimum triggering force for the 4-3 taper ratio

bistable metal strip; the 4-3 taper ratio was determined to have optimal performance (see above). Once the mentioned force was reached, the applied voltage was removed, and the Nitinol wire was allowed to cool. As can be seen in Figure S6(b), higher voltages applied to the Nitinol decreased the time required for the actuation force of 4.2 N to be reached, which indicated faster actuation. Although, the higher applied voltage led to an increase in the time required for the Nitinol to cool after removing the applied voltage. This could be explained considering the Joule heating effect. Assuming Ohm's Law applies, and the resistance of the Nitinol doesn't change during the process, when the voltage was higher, the current was higher, thus more heat was produced in a unit time, allowing the Nitinol to reach its phase transition temperature relatively fast. Although, this excess heat needs to be dissipated from the Nitinol wire to allow for its reversibility (Figure S6(c)). More detailed discussion and calculations are shown in **Figure S7**.

2.2.3. Actuation Durability

Durability, such as the number of times the Nitinol can contract/extend upon stimulation before failure, is an important parameter to study for the devices being generated here. Here, two sets of consecutive tests were performed using the same setup as in the previous actuation force test (Figure S6(a)). The voltage was applied for 10 s and removed to allow the Nitinol wire to cool. From **Figure 8**(a), we observed an ˜8.3% force decrease within the first 4 actuations, followed by a relative stabilization of the force decrease, i.e., an additional 14.8% decrease was observed after the subsequent 82 cycles. Then the same piece of Nitinol was used to determine its ability to reach the requisite 4.2 N force needed to trigger the 4-3 taper ratio bistable metal strip From Figure 8(b), we can see the Nitinol wire was able to reach 4.2 N after 222 repeats with no observable failure. Combining two consecutive tests, the Nitinol wire could at least endure 300 cycles of successful actuation. The exact number of cycles to reach failure was not investigated, but could be easily determined in the future.

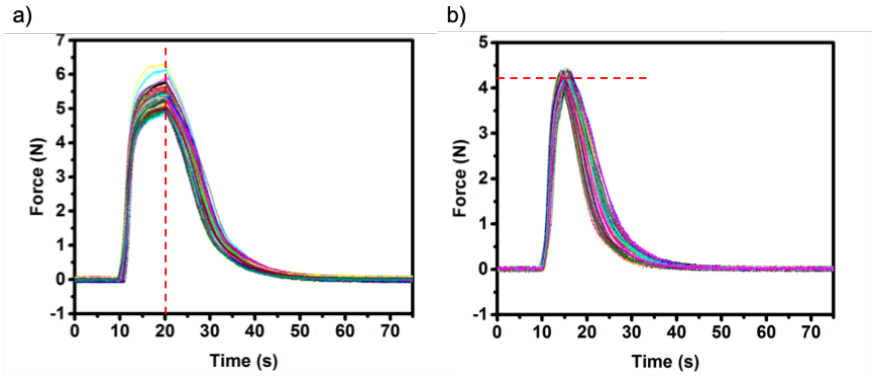

Figure 8: **a)** Force diagram of 10 seconds of actuation followed by cooling. Red dashed line represents roughly where the voltage is stopped. 86 repeats were performed. **b)** Force diagram of actuation until reaching 4.2 N (red dashed line) followed by cooling. 222 repeats were performed.

2.2.4. Under-Water Actuation

To generate a swimming device, it must be able to operate immersed in water at various water conditions, e.g., temperature and currents. One advantage of having water present is the quick cooling of the heated Nitinol compared to Nitinol in air. This is due to the fact that water has 4 times larger heat capacity and 25 times larger heat conductivity than air, which is beneficial for multiple consecutive actuations. However, the drawback is that water brings the Nitinol wire temperature down too quickly when the water temperature is low or when there is turbulence. Hence, we performed some actuation tests by immersing the Nitinol wire under water at room temperature and heating by application of a voltage. The results showed that a

much higher voltage was required to achieve similar Nitinol contraction compared to when the Nitinol was heated in air. Also, we can clearly see water convection on the surface of the Nitinol wire indicating quick and large heat loss (**Video S1**). With slight turbulence in the water, the Nitinol was not able to actuate at all, even at much higher voltage due to faster heat loss (**Video S2**), which made the actuation process unpredictable and uncontrollable. In order to hinder this heat loss process, and to provide the Nitinol wire with a stable, controllable and predictable actuation environment, we coated the Nitinol wire with a layer of polyacrylamide (PAAm) hydrogel (**Figure 9**(a)). A hydrogel was chosen as the coating material because it acts as a physical barrier to hinder the heat loss, but at the same time it can still dissipate the heat since it is a water-rich gel. As seen in Figure 9(b-c), with this hydrogel coating, the actuations were successfully observed and were stable even in turbulence while the one without hydrogel coating completely failed to actuate (**Video S3-S4**).

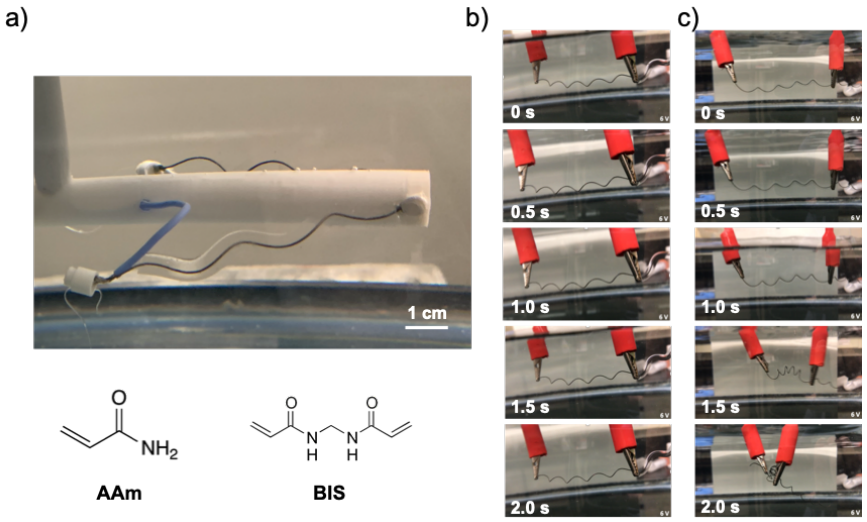

Figure 9: **a)** Polyacrylamide hydrogel coated Nitinol wires (bottom) monomer and crosslinker structures. Snapshots of Nitinol wire actuation under water **b)** without hydrogel coating **c)** with hydrogel coating (see Video S6/7).

2.3. Swimming Device

2.3.1. Assembly of the Device

The device was fabricated based on the aforementioned test results. The main body of the device was composed of a bistable metal strip with a pivot point going through the strip perpendicularly. Nitinol wires were connected at both tips of the metal strip against the pivot to set the angle required for triggering and resetting. A wireless control system was designed and assembled as shown in **Figure 10**(a). To increase the propelling ability, polydimethylsiloxane (PDMS) sheets with rigid plastic (3M PP2950 film) strips embedded were fabricated, which were inspired by fish fins. A lithium ion polymer battery was used as a portable power source.

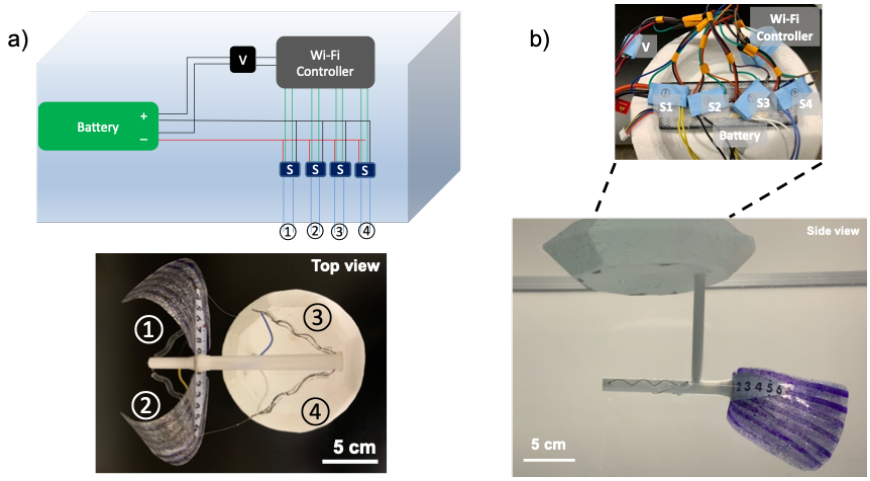

Figure 10: **a)** Illustration of the electronic components and (bottom) top view of the device. **b)** Device side view in water tank (top: electronic components; bottom: side view of the device).

2.3.2. Swimming Demonstration

Swimming behavior was achieved with wireless control and multiple swimming modes (**Video S5-S7**). The swimming device was immersed under water with a Styrofoam box floating on water carrying all the electronics (Figure 10(b)). By controlling the individual electronic switches, slow movement, and faster snapping actions could be realized. When both arms were working together, the swimming device could swim forward. When triggered to swim slowly, we determined the swimming speed to be 1.2 cm/s (**Video S8**), while it was increased to 5.5 cm/s upon triggering fast swimming (**Video S9**) (calculation see **Figure S8**). While with only one arm working, the device could turn. In the slow swimming speed regime, we observed the device could turn 180° within 10 seconds (**Video S10**). It should be noted here that the slow swimming speed is measured in two consecutive cycles with about 1.4 s time interval between the cycles and each actuation was about 0.3 s duration in terms of voltage application with 10% power output of the battery. Changes in time interval between cycles, voltage application time duration, and battery power output can all affect the slow swimming mode speed. The parameters can be manipulated and programmed easily. The fast swimming is measured after one single snapping movement and the speed is reproducible and decided due to the clear energy transform and release path. Some other factors like temperature of the water can also affect the swimming speed of the device. However, the overall swimming speed mainly depends on the time interval between cycles. Just like the octopus propelling their tentacles, more frequent the propelling, the faster the overall swimming speed. We can program the time interval between the cycles to control the speed of the swimming device. By combining different modes of actuation, the swimming device could easily navigate a water tank by swimming straight, speeding up, changing direction as well as slowing down.

2.4. Sensing Application

Microgel-based etalons were constructed by sandwiching poly(N-isopropylacrylamide) (pNIPAm)-based microgels between two thin Au layers. In addition to the native thermoresponsivity of pNIPAm, further responsivity can be imparted to microgels via copolymerization. For example, pNIPAm-based microgels can collapse and swell upon heating and cooling, respectively, while also exhibiting pH-and ionic strength-dependent solvation states by incorporating acrylic acid (AAc) into the pNIPAm microgels. Such responsive microgels in etalons allows their visual color, and peaks in reflectance spectra, to shift upon application of any of these stimuli, allowing the color to be correlated to the composition of the water, and its temperature. This is due

to the microgel solvation state mediating the distance between the etalon's Au layers, which are responsible for the etalon color; by changing the Au-Au distance, the color of the device changes. We can predict the etalons' optical properties by equation (1):

$$l = 2nd\cos j/m \tag{1}$$

where l is the wavelength of light being reflected, n is the refractive index of the microgel layer, d is the distance between the two Au layers (thickness of the microgel layer), ϑ is the angle of incident light, and m is the order of the reflected peak (e.g., 1, 2, 3,...). As mentioned above, the Au-Au distance (d) can be tuned by exposing the microgel-based etalons to different stimuli. In the work here, we focused on detecting pH and ionic strength changes, yielding a shift in the wavelengths of light reflected from the etalon, and a concomitant visual color change (Carvalho et al., 2021).

2.4.1. Device Integration

A 3D printed holder was made to accommodate etalon devices, a camera and a lighting system. The camera and lighting system was connected to the wireless control module and could take pictures of the etalons to monitor its color change as the water changes pH and ionic strength. The holder was attached to the Styrofoam boat body and immersed in water (**Figure 11**(a)).

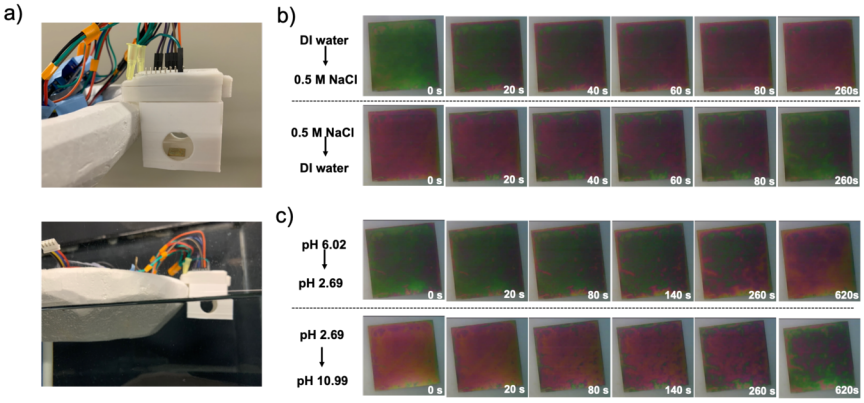

Figure 11: **a)** Pictures of 3D printed etalon holder and assembly (top: in air; bottom: in water). Photographs of etalons **b)** upon salt addition to water and **c)** a pH change.

2.4.2. Salt and pH Sensing

Etalons with salt and pH responsivity pNIPAm-co-10% acrylic acid (AAc)) were prepared following the group's previous fabrication procedure. After we change the solution media from deionized water (DI water) to 0.5 M sodium chloride (NaCl) solution, the color of the etalon chips changed from green to red in 260 s and could return back to green in 260s when put back to DI water (Figure 11(b)). Similarly, when the pH was changed from 6.02 to 2.69 , the color of the etalon chips changed from green to red in 620 s and could change from red to green in 620 s (Figure 11(c)). The swimming device served as a platform for different technologies and could potentially be applied in more research areas.

Conclusion

Our work first aim to present an innovative design using bistable metal strip and shape memory alloy Nitinol to fabricate a biomimetic actuator as a swimming device, which exhibited both slow moving and fast snapping capability like an octopus. We hope to inspire more research on combining different materials to achieve novel designs for more applications. Sensing application is just one of the many applications this device can achieve. Remote sampling collecting, video recording, humidity, temperature and air quality monitoring can all be potentially realized with thoughtful integration. Also, more complicated systems can be incorporated such as multiple devices working together as a team to improve efficiency. GPS and camera systems can be added to provide more flexible navigation and environment recognition capability. However, we do need to consider the long time memory loss of Nitinol wire after more repetitions, which was not exhaustedly investigated in this work. Future research should look into this and come up with an estimate time for Nitinol wire memory exhaustion. Also, how to recharge the battery when the device is far away in the field, and how to make sure we don't lose connection when battery runs out, etc. A straightforward solution might be adding solar panels, which can be a future improvement for the device. More importantly, bio-fouling can be a big challenge for devices that are deployed and immersed in water environment for long period of time. Special protective coatings or antifouling design for the device should be investigated.

In summary, a wirelessly controlled, programmable, swimming device was developed. The properties of the Nitinol alloy, bistable metal strips were investigated to find out optimum design. Hydrogel coating was chosen to provide a stable under-water environment for the Nitinol wires, which facilitates under-water actuation. A fish fin like PDMS flipper was also designed and increased the swimming ability. The swimming device could navigate in all directions and could be controlled wirelessly and easily programmable thanks to the untethered design with a portable battery and wireless control module. We also showcased its successful integration with an etalon-based sensing platform, which can potentially inspire more innovative future applications.

Experimental Section/Methods

Bistable Metal Strip Characterization: Bistable metal strips were purchased from Amazon (Seattle, Washington, USA), originally sold as slap/snap bracelets. We removed the plastic covers to obtain the metal strips with 21 cm in length, 2.5 cm in width and 0.15 mm in thickness. The metal strip has curvature on both long and short directions. The curvature for the long side is 1.5 cm and 2.4 cm for the short side. A pair of tin snips was used to cut the metal strips into different shapes with different taper ratios. A small hole was punctured on the tip of the metal strip to allow us to fix a piece of commercially available fishing thread (Beadalon Supplemax JNX0.25W-F, Coatesville, Pennsylvania, USA) with 0.01 inch diameter. We then screw a nail in the middle of the metal strip which acts as a pivot and allow its fixture on the clamp. The other end of the thread was fixed onto a force sensor (Vernier Dual-Range Force Sensor, Beaverton, Oregon, USA). A pulley was used to adjust and fix the force angles. Pull the thread until the metal strip snaps or resets and the forces are recorded in the Logger Pro software for later analysis.

Nitinol Wire Permanent Shape Setting: Nitinol wire with 0.02 inch diameter was purchased from McMaster-Carr (Elmhurst, Illinois, USA). The Nitinol wire was then coiled onto a 5 mm metal hex wrench with a pitch of 5 mm. The two ends were fixed using copper wire. Then we kept it inside a furnace (Thermolyne FB1315M, Thermo Scientific, Waltham, Massachusetts, USA) preheated to 510 for 30 min. Quickly chill it into room temperature (˜24) tap water until it's cooled.

Nitinol Wire Characterization: Nitinol phase transition temperature was tested both by DSC and water

bath test. 22.86 mg Nitinol sample was cut from the pre-set Nitinol coil. Mettler Polymer DSC (Mettler Toledo, Columbus, Ohio, USA) using STARe software (version 16.10) was used to perform DSC test by sweeping the temperature between 0 to 150 at a heating rate of 20 per minute. For the water bath test, we heated a beaker of water while monitoring the temperature. Stretch the coiled Nitinol wire, immerse it into a water bath at different temperatures and record the length change.

Nitinol actuation voltage and durability tests were done with the same setup. Pre-stretched Nitinol wire was fixed one end to a monkey bar, the other to a force sensor. Powerstat (Staco Energy Products Co. Type 3PN1010, Miamisburg, Ohio, USA) was used to deliver power. The on/off operations were performed by hands, which can be inconsistent between repeats. The actual on/off can be interpreted from the force/time graph.

Fabrication of PAAm Hydrogel-Coated Nitinol Wire Coil: All the chemicals were purchased from Sigma-Aldrich (St. Louis, Missouri, USA) and used as received. Milli-Q water was used unless otherwise stated. The PAAm hydrogel-coated Nitinol wire coil was fabricated by wrapping the hydrogel with a thin long channel in the middle onto the coiled-shaped Nitinol wire. First, prepare a pre-solution for hydrogel. Briefly, 0.5331 g of acrylamide (AAm) as monomer, 1.156 mg (0.1mol% of AAm) of N,N'-Methylenebis(acrylamide) (BIS) as crosslinker, and 13.5 mg of potassium persulfate (KPS) as initiator. Add DI water to afford a 2.5 mL solution mixture for later use. This formula was chosen based on many trails. The as prepared hydrogels are strong so they don't break easily but still have decent amount of water content. Also the hydrogels won't keep swelling and become too bulky and hinder the movement of the Nitinol. To prepare the long hydrogel with a thin channel inside, we used a commercially available fishing thread (Beadalon Supplemax JNX0.25W-F, Coatesville, Pennsylvania, USA) with 0.01 inch diameter as a template. A plastic tube with a 3.20 mm inner diameter was used. We horizontally clamped the plastic tube, put the fishing thread inside and fixed the two ends onto monkey bars. Then we pulled the thread to give it a bit tension to make sure it's straight inside the tube. The position of the tube and the thread was carefully adjusted so that the thread is going through the centre of the tube (**Figure S9**). Take 20 μL N,N,N',N'-Tetramethyl ethylenediamine (TEMED) as an accelerator and mix with the prepared pre-solution. Take some solution using a syringe and slowly inject it into the tube. After polymerization is completed and the hydrogel formed, slowly pull the thread to remove the hydrogel out of the tube. Then gently remove the thread inside which should leave a vacant channel inside. Lastly, slowly slide the Nitinol wire into the hydrogel through the channel.

Fabrication of PDMS Fish Fins: SYLGARD 184 Silicone Elastomer Kit from Dow Inc. (Midland, Michigan, USA) was purchased from Sigma-Aldrich. Mix polymeric base and curing agent at 10:1 ratio. Add some glitter powder (purchased from Dollarama, Montreal, Québec, Canada) and some crystal violet (Sigma Aldrich) for easy visualization under water. Mix well and pour the mixture into a large Petri dish. Put the Petri dish on a heating plate overnight at 65 . Cut a few 3 mm wide plastic strips from a piece of transparency film (3M PP2950, Saint Paul, Minnesota, USA). Place the strips onto the PDMS and pour another layer of PDMS pre-solution and cure overnight similar to previous steps. Cut the cured PDMS sheet into the fish fin shape. Attach the final fish fins onto the two ends of the bistable metal strip using superglue.

Design and Assembly of the Wireless Swimming Device: A lithium ion polymer battery (FCONEGY 11.1 V 3S 7000mAh 40 C Lipo RC Rechargeable Battery), a wireless Wi-Fi module with a camera (CANADUINO ESP32-CAM Wi-Fi Bluetooth Module with 2MP Camera), a voltage limiter (KeeYees MP1584EN Mini Step Down Buck Converter Adjustable DC to DC 4.5-28 V to 0.8-20 V Voltage Regulator Module) and four electronic switches (Mosfet Driver Module Dual High-Power 0-20 kHz FET PWM Trigger Switch Driver Module DC 5 V-36 V 15 A) were purchased from Amazon. One outlet from the battery was connected with the voltage limiter and then connected to the wireless Wi-Fi module. The Wi-Fi module was then connected to four electronic switches which are also powered directly by the battery through the second outlet. The electronic switches had wires to connect with the four pieces of Nitinol wires. The Wi-Fi module was programmed using Spyder 4.2.5 on Anacond-Navigator (**Figure S10**).

3D Printing of the Device Parts: The parts were designed using FreeCAD. Hollow design was adopted to hide the connecting wire in order to avoid cluster and keep the swimming device neat (**Figure S11**). Prusa

3D printer (Prusa Research Company, Prague, Czech Republic) was used for printing using polylactic acid (PLA) as the printing material.

Design and Assembly of the Sensing Platform: The holder was designed using FreeCAD and 3D printed using a Prusa 3D printer. The holder was then attached to the Styrofoam boat and adjusted so that the etalon chips could be fully immersed in water. The camera and LED lighting system were included in the wireless Wi-Fi module and were integrated and programmed into the whole control system so that the picture taking and lighting can work together to get good quality pictures.

alt and pH sensing: Etalons were fabricated based on previous procedure (**Figure S12**). For the salt response investigation, the swimming device was put into deionized water with the etalons fully immersed under water overnight. Pictures were taken to record the initial color. Then the media was then changed to 0.5 M NaCl solution, and pictures taken every minute to record the color change. Similarly, for pH sensing, pH 6.02 was used to record initial color. Then the media was adjusted to pH 2.69 and then 10.99. Color evolution was recorded by the camera system.

Acknowledgements

Michael J. Serpe acknowledges funding from the University of Alberta (the Department of Chemistry and the Faculty of Science), the Natural Sciences and Engineering Research Council of Canada (NSERC), the Canada Foundation for Innovation (CFI), and the Alberta Advanced Education & Technology Small Equipment Grants Program (AET/SEGP). Yu Wan acknowledges Alberta Innovates Technology Futures for a Graduate Student Scholarship.

Conflict of interest

All authors declare no financial/commercial conflicts of interest.

References

Cameron A Aubin, Snehashis Choudhury, Rhiannon Jerch, Lynden A Archer, James H Pikul, and Robert F Shepherd. Electrolytic vascular systems for energy-dense robots. *Nature*, 571(7763):51–57, 2019.

Bilge Baytekin, S Doruk Cezan, H Tarık Baytekin, and Bartosz A Grzybowski. Artificial heliotropism and nyctinasty based on optomechanical feedback and no electronics. *Soft robotics*, 5(1):93–98, 2018.

Marcello Calisti, Francesco Corucci, Andrea Arienti, and Cecilia Laschi. Dynamics of underwater legged locomotion: modeling and experiments on an octopus-inspired robot. *Bioinspiration & biomimetics*, 10 (4):046012, 2015.

Wildemar SP Carvalho, Cayo Lee, Yingnan Zhang, Adam Czarnecki, and Michael J Serpe. Probing the response of poly (N-isopropylacrylamide) microgels to solutions of various salts using etalons. *Journal of Colloid and Interface Science*, 585:195–204, 2021.

Paul Cazottes, A Fernandes, Joël Pouget, and Moustapha Hafez. Actuation of bistable buckled beams with macro-fiber composites. In *2008 IEEE/RSJ International Conference on Intelligent Robots and Systems*, pages 564–569. IEEE, 2008.

M Cianchetti, A Arienti, M Follador, B Mazzolai, P Dario, and C Laschi. Design concept and validation of a robotic arm inspired by the octopus. *Materials Science and Engineering: C*, 31(6):1230–1239, 2011.

Matteo Cianchetti, M Calisti, L Margheri, M Kuba, and C Laschi. Bioinspired locomotion and grasping in water: the soft eight-arm OCTOPUS robot. *Bioinspiration & biomimetics*, 10(3):035003, 2015.

Ming Dang, Laura Saunders, Xufeng Niu, Yubo Fan, and Peter X Ma. Biomimetic delivery of signals for bone tissue engineering. *Bone research*, 6(1):1–12, 2018.

T Duerig, A Pelton, and DJMS Stöckel. An overview of nitinol medical applications. *Materials Science and Engineering: A*, 273:149–160, 1999.

George B Kauffman and Isaac Mayo. The story of nitinol: the serendipitous discovery of the memory metal and its applications. *The chemical educator*, 2(2):1–21, 1997.

Asimina Kazakidi, Xenophon Zabulis, and Dimitris P Tsakiris. Vision-based 3D motion reconstruction of octopus arm swimming and comparison with an 8-arm underwater robot. In *2015 IEEE International Conference on Robotics and Automation (ICRA)*, pages 1178–1183. IEEE, 2015.

Zhenhua Li, Shiqi Hu, and Ke Cheng. Platelets and their biomimetics for regenerative medicine and cancer therapies. *Journal of Materials Chemistry B*, 6(45):7354–7365, 2018.

Yong Liu and Zeliang Xie. Detwinning in shape memory alloy. *Progress in smart materials and structures*, 3:29, 2007.

Philipp Rothemund, Alar Ainla, Lee Belding, Daniel J Preston, Sarah Kurihara, Zhigang Suo, and George M Whitesides. A soft, bistable valve for autonomous control of soft actuators. *Science Robotics*, 3(16), 2018.

Courtney D Sorrell and Michael J Serpe. Reflection order selectivity of color-tunable poly (N-isopropylacrylamide) microgel based etalons. *Advanced materials*, 23(35):4088–4092, 2011.

George M Whitesides. Bioinspiration: something for everyone. *Interface focus*, 5(4):20150031, 2015.

Hua Ye and Sergio Pellegrino. Bi-stable space frames. In *46th AIAA/ASME/ASCE/AHS/ASC Structures, Structural Dynamics and Materials Conference*, page 1870, 2005.